SYNTHESIS STRUCTURAL AND PHYSICAL PROPERTIES OF BaFeO$_{3-\delta}$ PEROVSKITES

HANANE FODIL, MAHMOUD OMARI

Laboratory of Molecular Chemistry and Environment, University of Biskra, B.P 145, 07000 Biskra, Algeria

RESUME

Les matériaux pérovskites BaFeO$_{3-\delta}$ ont été synthétisés par la méthode de l'acide citrique (sol-gel). L'analyse par la diffraction X (DRX) indique que BaFeO3-δ calciné à 850 ° C présente une structure hexagonale qui se transforme à une structure rhomboédrique à 1000 ° C. Pendant la calcination du catalyseur précurseur, une série de réactions solides complexes se déroulent, et la BaCO$_3$, formé lors de la combustion de l'acide citrique, a joué un rôle clé pour réagir avec les phases spinelles donnant la pérovskite. Pour le catalyseur BaFeO3-δ, la phase pérovskite et la petite quantité de phase spinelle sont mises en évidence par DRX, alors que le carbonate bien dispersé a été détectées par FT-IR. La microstructure et la morphologie du composé montrent que les poudres sont constituées par l'agrégation de particules de différentes dimensions et formes.

MOTS CLES: oxydes pérovskites; méthode sol-gel; analyse DRX; analyse thermique.

ABSTRACT

BaFeO$_{3-\delta}$ perovskite materials have been synthesized by citric acid sol–gel method. Powder XRD indicates a hexagonal structure for BaFeO$_{3-\delta}$ calcined at 850°C with a change to a rhombohedral perovskite at 1000°C. During the catalyst precursor calcination, a series of complex solid reactions happened, and the BaCO$_3$, formed during citric acid combustion, played a key role to react with the spinel species achieving the aimed perovskite. On the BaFeO$_{3-\delta}$ catalyst, the perovskite phase and the small amount of spinel phase were evidenced by XRD, and some well dispersed carbonate was also detected by FT-IR. The microstructure and morphology of the compound show that the powders are constituted by the aggregation of various dimensions and forms of particles.

KEYWORDS: perovskite oxide; sol-gel method; powder XRD; thermal analysis.

1 INTRODUCTION

In recent years, ABO$_3$ perovskite-type oxides were widely researched focused on their excellent defect structure, [1] superior catalytic activity, [2, 3] well thermal stability [4], and other superior properties [5-7]. The activity of ABO$_3$ perovskite-type oxides is ascribed to two main characteristics. (1) The corner-shared octahedron BO$_6$ network facilitates electron transfer and oxygen transfer, leading to the oxygen non-stoichiometry [8-12], making ABO$_3$ an excellent catalyst for degradation of pollutant [13], and inducing ABO$_3$ to exhibit high reducibility [14]. (2) The large atoms at A-site of ABO$_3$ contribute to the stabilization of perovskite structure [15-18]. Then structure of ABO$_3$ oxides can become more active and the electrons can be excited easily by external energy such as light irradiation and transfer easily. However, perovskite structure is flexible and shows an allowable distortion or shows metastability with the existence of vacancy [19, 20]. The variation of oxygen vacancy is crucial to the activity and stability of ABO$_3$ perovskite type oxides [21]. So far, there have been some investigations focused on the activity of BaTiO$_3$ or BaFeO$_3$ in gas-phase [22, 23] but there are few investigations focused on the application of BaMO$_{3-\delta}$ type (M = transition metal atom, such as Ti, Fe and Co) perovskite in liquid-phase. Barium ferrite as a ferromagnetic material [24, 25] exhibit excellent chemical stability and corrosion resistivity in gas phase. But the stability and corrosion resistivity of perovskite-type alkaline earth oxides seems not well in wet environment [17, 26-27]. For (Ca$_x$Sr$_{1-x}$)(Co$_y$Fe$_{1-y}$)O$_{3-\delta}$ perovskite, in its applied research for CO$_2$ absorption [28]. It was found that the concentration of Sr, Ca vacancies increases with the higher absorbed CO$_2$ concentration. And other related investigations indicated that related hexavalent iron compounds are unstable under ambient conditions [26, 29-

30].

One alternative approach to enhance the stability of perovskite ferrite refers to isovalent doping into the Fe sublattice with trivalent cations having stable oxidation state, such as Ga or Al [31-35]. In the system $(La,Sr)(Fe,Ga)O_{3-\delta}$, the maximum level of oxygen ionic conductivity, essentially independent of the oxygen nonstoichiometry and vacancy ordering in a wide range of the oxygen partial pressure from 10-20 Pa to 21278,25 Pa, was found for the $La_{0.3}Sr_{0.7}Fe_{1-x}Ga_xO_{3-\delta}$ series [31-32,35-36]. Furthermore, incorporation of gallium into the iron sublattice was shown to suppress unfavorable thermal and chemically induced expansion of the perovskite lattice [37]. The Ga-substituted ferrites possess, however, a number of specific disadvantages including volatilization of gallium oxide in reducing atmospheres [38], possible interaction with catalysts such as Pt or Ni [38,39] and high cost of Ga containing grew materials.

In this study, the perovskite type $BaFeO_{3-\delta}$ catalyst was prepared by sol–gel method. The preparation technique, thermal behavior, crystal structure, The microstructure and morphology of the compound, behavior of the low-temperature synthesized $BaFeO_{3-\delta}$ nanopowders have been discussed in detail.

2   EXPERIMENTAL PROCEDURE

2.1   Synthesis

$BaFeO_{3-\delta}$ oxide was prepared by a sol-gel method using citric acid as a complexing agent. Aqueous solutions of $Ba(NO_3)_2$ (PANREAC 99%), $Fe(NO_3)_3.9H_2O$ (BIOCHEM 98.5%) and were first dissolved in absolute formaldehyde (methanal) separately. The molar amount of citric acid was equal to total molar amount of metal nitrates in solution. Citric acid (Biochem) was added to the precursors under vigorous stirring. The homogeneous solution obtained was heated at 80-90 °C for 4 h.To remove the solvent, the gel is heated for 24 h at 100 °C. The resulting precursor is then milled and calcined in air for 6 h at different calcination temperatures: 400, 600, 700, 800, 850,900, 950 and 1000 °C with a heating rate of 5 °C min^{-1}.

2.2   Characterization Techniques

The thermal decomposition processes of the precursor gels were studied in air atmosphere by TGA Schimadzu with a heating rate of 10 °C/min in air, from room temperature to 1000°C.

Infrared transmission spectra were performed on a Fourier transform spectrometer (FTIR) Shimadzu 8400S. A granular technique employing KBr (1 mg of sample added to 200 mg of KBr) was used, and the spectra were recorded in the 400–4000 cm^{-1} range.

X rays diffraction (XRD) patterns were collected on a Bruker AXS D8 advance diffractometer employing Cu Ka radiation. In all diffractograms, a step size of 0.02° (2θ)

was used with a data collection time of 15 s. Data were collected between 2θ values from10° to 80° using standard θ/2θ geometry. Identification of crystalline phases was carried out by comparison with JCPDS standards. The unit cell parameters were obtained by fitting the peak position of the XRD pattern using the CELREF and X'pert Highscore programs. Moreover, morphological aspects of the powders were examined by using a ESEM-FEI Quanta 600 FEG scanning electron microscope (SEM).

3   RESULTS AND DISCUSSION

3.1   Thermogravimetric Analysis

The precursors $BaFeO_{3-\delta}$ (after the drying step of the preparation at 100 °C) were examined by TGA in order to explore her decomposition under atmospheric air and with the aim of establishing most adequate calcination conditions for her. The results are shown in Fig.1. This profile is characterized by four significant weight loss stages at the temperature ranges of 25-180, 180-350, 350-640 and 640-930 °C. A first weight loss in the temperature range between 25-180, which must be related to the desorption of adsorbed or hydration water may remain in the precursors [40]. The second one represents an important mass loss (ca. 27 %) and takes place between ca.180 and 350 °C. Such mass loss appears consistent with the oxidative decomposition of citrates complexing the metals in the precursors [41]. The third one takes place between ca. 350 and 640 °C and corresponds to a mass loss of about 17 %. It could be related to the decomposition of carbonate or carboxylate-type complexes remaining in the samples, as will be confirmed below. The final process occurs between 640 and 930 °C and must correspond to the crystallization of the oxides, as will be confirmed below, along with the slow decomposition of more persistent residual carbonate- or carboxylate-type species [41]. Above 930 °C a slight weight loss were observed, which can be possibly attributed to the change in crystal structure, and the oxygen loss in the system.
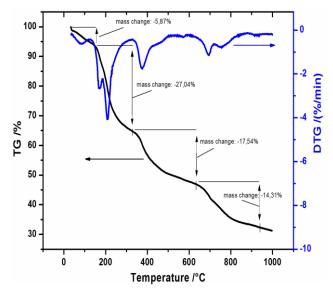
Figure 01: Thermogravimetric profiles of BaFeO$_{3-\delta}$ precursor

Figure 02: XRD patterns of the BaFeO$_{3-\delta}$ powder calcined at different temperatures: (c) BaCO$_3$; (P) hexagonal phase; (S) BaFe$_2$O$_4$; (B) rhombohedral phase

3.2 X Ray diffraction

XRD experiments were first performed to check the phase purity of the materials. Figure 2 shows the XRD patterns of BaFeO$_{3-\delta}$ calcined at different temperatures for 6 h. After calcination at 400 and 600 °C, the precursor is a mixture containing orthorhombic BaCO$_3$ (PDF: 05-0378) and spinel BaFe$_2$O$_4$ (PDF: 46-0113). When the precursor was heated over 700 °C in air for 6 h, the characteristic diffraction peaks of BaCO$_3$ and BaFe$_2$O$_4$ decrease and become weaker at 800°C, while those of hexagonal perovskite structure appear. At 850°C the intensity of characteristic diffraction peaks of hexagonal perovskite becomes stronger and no reflections from barium oxide are observed as distinct intermediate phases to the formation of BaFeO$_{3-\delta}$ during the thermal decomposition of the precursor powder. With further increase in calcination temperature above 900 °C the main intensive peak at 31° split into multiple peaks between 30.9 and 31.9° indicating the change in crystal structure, which was due to the transformation from hexagonal perovskite to rhombohedral perovskite (PDF: 00-020-0130). This is consistent with TGA. This change should be ascribed to the oxygen loss and the formation of oxygen vacancy [27, 40].
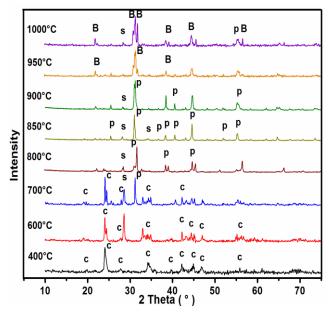
3.3 IR Spectroscopy

The vibration frequencies in the infrared region are fundamental for the control of the reaction process and properties of materials. The FTIR spectra of BaFeO$_{3-\delta}$ precursor and calcined powder at different temperatures recorded in the range of 400-4000 cm^{-1} are shown in Fig 3. To clarify the formation process of the BaFeO$_3$ perovskite catalyst, A broad absorption in the spectrum of the precursor powder at around 3300 cm^{-1} are probably related to the stretching vibration of the free hydroxyl group which indicates also the presence of adsorbed water [41], this band gradually decreases with the temperature increase. For the precursor calcined at 400, 600 and 700°C bands were observed at 1430, 850, 780, 625 and 490 cm^{-1}. The sharp absorption band at 1430 cm^{-1} is due to the stretch vibrations in carbonate [27, 40]. The absorption peak at 850 cm-1 marks the existence of BaCO$_3$ [27]. These bands disappear with increasing temperature, suggesting the decomposition of the residual material of the synthesis process. However the peak at 780 cm-1 marks the formation of BaFe$_2$O$_4$ spinel [27, 40, 42]. The BaFeO$_{3-\delta}$ perovskite generates when calcined at 850 °C, with the absorption peaks at 490 and 625cm^{-1} marking the formation of FeO$_6$ in BaFeO$_{3-\delta}$ [27, 40]. With the calcination temperature further increasing to 1000 °C, the peaks 490 and 625cm^{-1} become more obtuse. This result further consisted in the finding of increase in oxygen loss in XRD patterns analysis. Considering the higher mobility of oxygen in perovskite structure, for BaFeO$_{3-\delta}$, the oxygen loss occurs gradually with the calcination temperature further increasing to 1000°C and above, and then the oxygen vacancy forms. The oxygen loss is due to the thermal excitation under the higher calcination temperature [42].
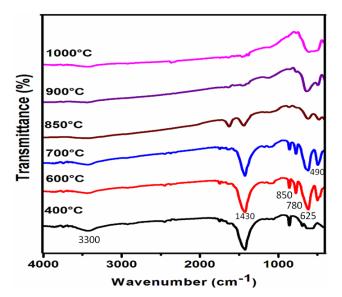
Figure 03: FTIR spectra of BaFeO₃₋δ powder calcined at different temperatures

Figure 04: Crystallite size of BaFeO₃₋δ powders calcined at different temperatures for 6 h

3.4 Structural and Morphological Characterization

The peak broadening at lower angle is more meaningful for the calculation of particle size, therefore size of nanocrystals. The crystallite size (D) of the samples was calculated from the full width at half maximum of the most intense diffraction peak using Scherrer's equation (Eq. 1): [43].

$$D = 0.89\lambda / \beta\cos\theta \qquad (1)$$

Where D is the mean crystallite size, ß is the full width at half maximum and λ is the used radiation wavelength (1.54059 Å) and θ is Bragg's diffraction angle.

Figure. 4 shows the variation of average crystallite size (D_{XRD}) of the BaFeO₃₋δ powders calcined at different temperatures for 6 h. The crystallite sizes calculated from the Scherrer formula are slightly increase in the range of 53.2–69.50 nm respectively with the calcination temperature increasing from 700 to 900°C. This distinction can be caused of synthesis parameters such as chemical nature of the base solvent that affects on the morphological characteristics of the nanoparticles BaFeO₃₋δ powders.
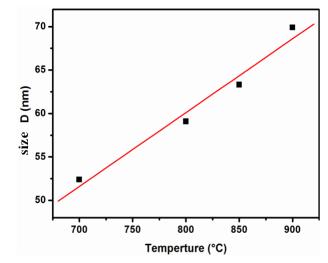
The SEM micrographs of the BaFeO₃₋δ compound are shown in Fig 5. A different surface morphology for all samples is observed. Particles are large and have an inhomogeneous dispersion of particle sizes. The powder is constituted by the aggregation of various dimensions and forms of particles with the grain size greater than 1μm. The formation of agglomerate is probably due to the nature of the solvent used in the preparation of the precipitate. The same result was also found for samarium-doped ceria powders [44], and $SrCo_{1-x}N_ixO_{3-\delta}$ oxides [45]. It has been shown that treating the precipitate with water and ethanol allows interactions between particles which leads during drying to the formation of chemical bonds.
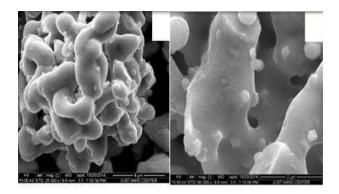

Figure 05: SEM micrographs of BaFeO₃₋δ

4 CONCLUSION

The BaFeO₃₋δ perovskite family was prepared via a sol–gel method. TGA–DTA and XRD analysis of the decomposition of the precursors show that minimum temperature to achieve full crystallization of the components is 850 °C. The nanocrystallite size slightly increase from 53.2 to 69.5 nm with the calcination temperature increasing from 700 to 900°C, for the BaFeO₃₋δ precursor powders calcined for 6 h. The microstructure and

morphology of the compounds show that the powders are constituted by the aggregation of various dimensions and forms of particles.

5   ABRÉVIATIONS DÉFINITIONS

VO.. Lacune d'oxygène
βk Largeur du rectangle
S (cm²) Surface de l'échantillon
ϑ (°) Angle de Bragg
λ (Å) Longueur d'onde du rayonnement
F (96500 C/ mole) Faraday constante
C (mol.cm⁻³) Concentration (mol /ml)
BaFeO₃ Oxyde de ferrite de baryum
ABO₃ Oxydes type pérovskite
A.T.G Analyse thermogravimétrique
A.T.D Analyse thermique différentielle
d (hkl) distance entre les plans réticulaires
a, b, c Paramètre de maille de la structure pérovskite
V (Å) Volume de maille
α, β et γ angles formés
D Taille moyenne des Cristallites nm
DRX Diffraction des rayons X
FT-IR Spectroscopie Infrarouge à transformée de Fourier
MEB Microscopie électronique à balayage
S (cm²) Surface de l'échantillon

REFERENCES

[1] Y Ueda, N Nakayama 1998, Solid State Ionics 108 303-306.

[2] N Gunasekaran, N Bakshi, C B Alcock, J J Carberry 1996, Solid State Ionics 83 145-150.

[3] H Taguchi, Y Masunaga, K Hirota, O Yamaguchi 2005, Mater. Res. Bull 40 773-780.

[4] K D Kreuer 1999, Solid State Ionics 125 285-302.

[5] Y Hu, O K Tan, J S Pan, H Huang, W Cao 2005, J Sens. Actuators, B 108 244-249.

[6] A Mai, V A C Haanappel, S Uhlenbruck, F Tietz, D Stover 2005, Solid State Ionics 176 1341–1350.

[7] Y Teraoka, H Shimokawa, C Y Kang, H Kusaba, K Sasaki 2006, Solid State Ionics 177 2245–2248.

[8] M James, T Tedesco, D J Cassidy, R L Withers 2005, Mater Res Bull 40 990-1000.

[9] Z Q Deng, W Liu, D K Peng, C S Chen, W S Yang 2004, Mater Res Bull 39 963-969

[10] C Duque, A Stashans 2003, J Physica B 336 227–235

[11] J C Grenier, A Wattiaux, M Pouchard, P Hagenmuller, M Parras, M Vallet, J Calbet, M A Alario-Franco 1989, J Solid State Chem 80 6–11.

[12] J M Gonzalez-Calbet, M Parras, M Vallet-Regi, J C Grenier 1990, J Solid State Chem 86 149–159.

[13] R Spinicci, A Delmastro, S Ronchetti, A Tofanari 2002, J. Mater Chem Phys 78 393–399.

[14] J L G Fierro, J M D. Tascon, L G Tejuca 1985, J Catal 93 83–91.

[15] J Kubo, W Ueda 2009, Mater Res Bull 44 906–912.

[16] O Haas, U F Vogt, C Soltmann, A Braun, W S Yoon, X Q Yang, T Graule 2009, Mater Res Bull 44 1397–1404.

[17] G Pecchi, C Campos, O Pena 2009, Mater Res Bull 44 846–853.

[18] A K Azad, A Khan, S G Eriksson, J T S Irvine 2009, Mater. Res. Bull. 44 2181–2185.

[19] K Rida, A Benabbas, F Bouremmad, M A Pena, E Sastre, A Martınez-Arias 2007, J Appl Catal A 327 173–179.

[20] G C M Rodrıguez, R Ochrombel, B Saruhan 2008, J Eur Ceram Soc 28 2611-2616.

[21] H J Van Hook 1964, J Phys Chem 68 3786-3789.

[22] J H Kim, S H Yoon, Y H Han 2007, J Ceram Soc 27 1113-1116.

[23] J Hombo, Y Matsumoto, T Kawano 1990, J Solid State Chem 84 138–143.

[24] R C Pullar, A K Bhattacharya 2002, J Mater Lett 57 537–542.

[25] J Dho, E K Lee, J Y Park, N H Hur 2005, J Magn Magn Mater 285 164-168.

[26] [26] I Nowik, R H Herber, M Koltypin, D Aurbach, S Licht 2005, J Phys Chem Solids 66 1307-1313.

[27] Y Yang, Y Jiang, Y Wang, Y Sun 2007, J Catal A Chem 270 56-60.

[28] K Suvegh, K Nomura, G Juhasz, Z Homonnay, A Vertes 2000, J Radiat Phys Chem 58 733-736.

[29] J Madarasz, R Zboril, Z Homonnay, V K Sharma, G Pokol 2006, J Solid State Chem 179 1426-1433.

[30] S Svarcova, K Wiik, J Tolchard, H J M Bouwmeester, T Grande 2008, Solid State Ionics 178 1787–1791.

[31] V V Kharton, A A Yaremchenko, A P Viskup, M V Patrakeev, I A Leonidov, V L Kozhevnikov, F M Figueiredo, A L Shaulo, E N Naumovich, F M B Marques 2002, J. Electrochem. Soc 149 125-135.

[32] V V Kharton, A L Shaulo, A P Viskup, M Avdeev, A A Yaremchenko, M V Patrakeev, A I Kurbakov, E N Naumovich, F M B Marques 2002, Solid State Ionics 150 229-243.

[33] M Schwartz, J H White, A F Sammells 2001, US patent 6 214-757.

[34] J T Ritchie, J T Richardson, D Luss 2001, AIChE J. 47 2092.

[35] M V Patrakeev, E B Mitberg, A A Lakhtin, I A Leonidov, V L Kozhevnikov, V V Kharton, M Avdeev, F M B Marques 2002, J. Solid State Chem 167 203-213.

[36] I A Leonidov, V L Kozhevnikov, E B Mitberg, M V Patrakeev, V V Kharton, F M B Marques 2001, J. Mater. Chem 11 1201.

[37] V V Kharton, A A Yaremchenko, M V Patrakeev, E N

Naumovich, F M B Marques 2003, J. Eur. Ceram. Soc 23 1417-1426.

[38] K Yamaji, T Horita, M Ishikawa, N Sakai, H Yokokawa 1999, Solid State Ionics 121 217-224.

[39] P Huang, A Horky, A Petric 1999, J. Amer. Ceram. Soc 82 2402-2406.

[40] H Xian, X Zhang, X Li, H Zou, M Meng, Z Zou, L Gou, N Tsubaki 2010, J. Catal. Today 158 215-219.

[41] K Rida, M A Pena, E Sastre, A Martinez-Arias 2012, J Rare Earths 30(3):210-216.

[42] M Sun, Y Jiang, F Li, M Xia, B Xue, D Liu 2010, J. Mater. Trans 51 1981 -1989.

[43] H Xiao, Ch Xue, P 0 Song, J Li, Q Wang 2015, J. Appl. Surf. Sci. doi org / 10 .1016 / j. apsusc 2015 02 064.

[44] G B Jung, T J Huang, M H Huang, C L Chang 2001, J. Mater. Sci 36 5839.

[45] S Makhloufi, M Omari 2016, J Inorg Organomet Polym 26 32-40.